BAMS Article

Advanced Quantitative Precipitation Information

Improving Monitoring and Forecasts of Precipitation, Streamflow, and Coastal Flooding in the San Francisco Bay Area

Rob Cifelli, V. Chandrasekar, L. Herdman, D. D. Turner, A. B. White, T. I. Alcott, M. Anderson, P. Barnard, S. K. Biswas, M. Boucher, J. Bytheway, H. Chen, H. Cutler, J. M. English, L. Erikson, F. Junyent, D. J. Gottas, J. Jasperse, L. E. Johnson, J. Krebs, J. van de Lindt, J. Kim, M. Leon, Y. Ma, M. Marquis, W. Moninger, G. Pratt, C. Radhakrishnan, M. Shields, J. Spaulding, B. Tehranirad, and R. Webb

KEYWORDS:
Complex terrain;
Flood events;
Precipitation;
Storm surges;
Hydrology;
Forecasting

ABSTRACT: Advanced Quantitative Precipitation Information (AQPI) is a synergistic project that combines observations and models to improve monitoring and forecasts of precipitation, streamflow, and coastal flooding in the San Francisco Bay Area. As an experimental system, AQPI leverages more than a decade of research, innovation, and implementation of a statewide, state-of-the-art network of observations, and development of the next generation of weather and coastal forecast models. AQPI was developed as a prototype in response to requests from the water management community for improved information on precipitation, riverine, and coastal conditions to inform their decision-making processes. Observation of precipitation in the complex Bay Area landscape of California's coastal mountain ranges is known to be a challenging problem. But, with new advanced radar network techniques, AQPI is helping fill an important observational gap for this highly populated and vulnerable metropolitan area. The prototype AQPI system consists of improved weather radar data for precipitation estimation; additional surface measurements of precipitation, streamflow, and soil moisture; and a suite of integrated forecast modeling systems to improve situational awareness about current and future water conditions from sky to sea. Together these tools will help improve emergency preparedness and public response to prevent loss of life and destruction of property during extreme storms accompanied by heavy precipitation and high coastal water levels—especially high-moisture laden atmospheric rivers. The Bay Area AQPI system could potentially be replicated in other urban regions in California, the United States, and worldwide.

https://doi.org/10.1175/BAMS-D-21-0121.1
Corresponding author: Rob Cifelli, rob.cifelli@noaa.gov
In final form 1 October 2022

AFFILIATIONS: Cifelli, White, Gottas, and Webb—NOAA/Physical Sciences Laboratory, Boulder, Colorado; **Chandrasekar, Chen, Junyent, Ma, and Radhakrishnan**—Cooperative Institute for Research in the Atmosphere, Fort Collins, Colorado; **Herdman, Barnard, Erikson, and Tehranirad**—USGS Pacific Coastal and Marine Science Center, Santa Cruz, California; **Turner, Alcott, Marquis, and Pratt**—NOAA/Global Systems Laboratory, Boulder, Colorado; **Anderson**—California Department of Water Resources, Sacramento, California; **Biswas, Johnson, and Kim**—NOAA/Physical Sciences Laboratory, Boulder, and Cooperative Institute for Research in the Atmosphere, Fort Collins, Colorado; **Boucher**—Contra Costa County Public Works, Concord, California; **Bytheway**—NOAA/Physical Sciences Laboratory, and Cooperative Institute for Research in Environmental Sciences, Boulder, Colorado; **Cutler, van de Lindt, and Shields**—Colorado State University, Fort Collins, Colorado; **English, Leon, and Moninger**—NOAA/Global Systems Laboratory, and Cooperative Institute for Research in Environmental Sciences, Boulder, Colorado; **Jasperse and Spaulding**—Sonoma Water, Santa Rosa, California; **Krebs**—Jennifer Krebs Environmental Planning, Berkley, California

Wintertime precipitation is vital for replenishing snowpack and filling reservoirs in the western United States. Along the U.S. West Coast, much of the wintertime precipitation comes from atmospheric rivers (ARs), which are narrow bands of concentrated water vapor transport often associated with landfalling extratropical cyclones (Zhu and Newell 1998). Nearly half of California's annual precipitation comes from a handful of AR events (Dettinger et al. 2011). ARs and their accompanying heavy rains can be both good news and bad news for California residents: they can bring relief for anxious water managers in a drought-prone region. However, that much water—arriving over a period of several days or less—can cause major flooding, endangering lives and property. ARs are responsible for more than 80% of the flood damages in the western United States, including California, with over $1 billion in average annual costs (Corringham et al. 2019).

The San Francisco Bay Area is particularly prone to significant flooding and the resulting damage from ARs (Corringham et al. 2019). Recent examples in the Bay Area include flooding impacts from a series of rain events in February 2017 which caused flood damage in the city of San Jose, as Coyote Creek overflowed its banks and inundated neighborhoods forcing 14,000 residents to evacuate. This series of rain events was also responsible for severe damage to the Oroville Dam spillway and an evacuation of nearly 200,000 residents downstream of the dam (White et al. 2019). All told, the February 2017 storms were responsible for over $1.5 billion in damages (NCEI 2021). In 2019, another series of Bay Area rainfall events resulted in over $150 million in flood damages and a presidential disaster declaration (FEMA 2019a,b). Landslides can also be a potential hazard. Cordeira et al. (2019) showed that the vast majority of landslides in the San Francisco Bay Area were associated with ARs.

The complex terrain and the proximity of San Francisco Bay makes this region susceptible to flooding events. Flash flooding along inland rivers and creeks that drain hundreds of small watersheds can combine with coastal flooding along the bay shoreline to exacerbate the overall magnitude of an event, producing compound flooding events. Urbanization is also a contributing factor. This area is home to more than 7 million people, encompassing nine counties, three major cities (San Francisco, Oakland, and San Jose), and adjacent communities. According to a recent report from the California Department of Water Resources (CA DWR 2013), nearly 400,000 people in the Bay Area are exposed in the 100-yr floodplain.

Impervious surfaces and stormwater runoff can exacerbate flooding conditions. The urban impacts from flooding range from degraded water quality in the Bay to flooded roadways and buildings during storms. Sea level rise and continued urbanization in the region is expected to amplify the problem.

The rugged terrain in the San Francisco Bay Area makes it especially challenging to monitor and forecast extreme rain and subsequent flooding events. Existing weather monitoring infrastructure—satellites, offshore observations, and the operational radar network (NEXRAD; Crum and Alberty 1993)—have enabled forecasters to provide notice of rain events, and ascertain their severity, much of the time. The forecasts, though, have not always provided specificity sufficient enough to guide actions that could be taken to offset damaging impacts. The reason is that precipitation often forms or is enhanced in very low levels of the atmosphere, below the level that the existing NEXRAD network can see well, through orographic lifting and warm rain collision–coalescence processes (White et al. 2003). Additionally, the observations of some of the radars in the Bay Area are blocked by coastal mountains, leaving blind spots in the observation network.

The CA DWR and the U.S. Department of Energy have invested in a "picket fence" of atmospheric river observatories (AROs) along the U.S. West Coast to monitor wind and temperature profiles, column-integrated water vapor, onshore moisture flux, and freezing elevation at seven coastal sites and two inland sites[1] (White et al. 2015; Ray and White 2019). The AROs, built by the National Oceanic and Atmospheric Administration Physical Sciences Laboratory (NOAA/PSL), have been used routinely to initialize and evaluate forecasts made by the National Weather Service (NWS). The system also enables water resources managers to gauge the intensity of an AR event at the location of the ARO. They do not, however, scan like a typical weather radar. Rather, AROs view the atmosphere directly above them in fine detail. Scanning radar is needed to fill in the gaps between AROs to detect variations in storms across different watersheds. A NOAA-supported, pre-AQPI temporary deployment of a scanning radar system in Santa Clara, California, was able to demonstrate improved high-resolution rainfall estimates (Cifelli et al. 2018).

[1] The inland ARO site within the AQPI domain at Twitchell Island, California, does not measure temperature profiles, but it has a precipitation profiling radar and surface-based disdrometer to provide microphysical measurements of the precipitation observed at that site.

The purpose of this article is to provide an overview of the Advanced Quantitative Precipitation Information (AQPI) Project. The AQPI Project was awarded by CA DWR to NOAA and contributing partners in 2017 and is administered by the Sonoma Water Agency. AQPI was designed to obtain more precise measurements and forecasts of precipitation, streamflow, and coastal flooding in the San Francisco Bay Area. The concept was developed in response to requests from the Bay Area water management community for higher-temporal- and spatial-resolution information than was currently available to guide their decision-making for water management and flood response operations. The origins of AQPI trace back over a decade, building on fundamental research to improve understanding of hydrometeorological processes conducted through NOAA's Hydrometeorology Testbed (Neiman et al. 2002; White et al. 2003; Matrosov et al. 2005; Zhang et al. 2012; Sumargo et al. 2020) with support from CA DWR and the Sonoma Water Agency. One of the strengths of AQPI is the collaborative approach between local, state, and federal agencies. Table 1 lists agencies involved in AQPI and their roles in the project.

AQPI components

AQPI includes a combination of integrated observations and high-resolution model forecasts to track storm systems as well as to predict precipitation, streamflow, and coastal flooding across the Bay Area (Fig. 1). As noted above, the foundation for AQPI observations builds on an existing network established by NOAA, CA DWR, Scripps Institute of Oceanography,

Table 1. Agencies involved in AQPI and their role.

Agency	Role
NOAA Physical Sciences Laboratory	Program technical lead; quantitative precipitation estimation (QPE) development and evaluation; precipitation and streamflow forecast evaluation; surface meteorology and profiler sites; benefits evaluation
NOAA Global Systems Laboratory	AQPI system development; High-Resolution Rapid Refresh (HRRR) model development and evaluation
NOAA Cooperative Institute for Research in the Atmosphere	Radar install, testing, operation; QPE and nowcast development, testing, and evaluation
NOAA Cooperative Institute for Research in Environmental Sciences	HRRR simulations and evaluation; QPE uncertainty
USGS Pacific Coastal and Marine Science Center	Coastal Storm Modeling System (CoSMoS) development, testing, and operation
NOAA National Severe Storms Laboratory	Integration of AQPI radar data into Multi-Radar Multi-Sensor (MRMS)
Colorado State University Department of Economics	AQPI benefits analysis
Scripps Institute of Oceanography	Development of long-term concept of operations for AQPI
CA DWR	Grant sponsor
Sonoma Water	Grant administrator, facilitate interaction with local partners, radar siting, product evaluation and feedback
Valley Water	Hosting X band; data provider; AQPI product evaluation and feedback
San Francisco Public Utilities	Hosting X band; data provider; AQPI product evaluation and feedback
Contra Costa County	Cohosting and infrastructure support for X band; data provider; AQPI product evaluation and feedback
East Bay Municipal	Cohosting X band; data provider; AQPI product evaluation and feedback
Alameda County	Cohosting X band; data provider; AQPI product evaluation and feedback
Napa County	AQPI product evaluation and feedback
Marin County	AQPI product evaluation and feedback
National Weather Service	AQPI product evaluation and feedback

San Jose State, and Sonoma Water to monitor extreme precipitation in California. The coastal modeling component also builds upon work done in and around San Francisco Bay by the USGS and collaborators (Nederhoff et al. 2021; Tehranirad et al. 2020; Martyr-Koller et al. 2017).

The core foundation of AQPI observations are new radar systems: four X band and one C band as shown in Fig. 2 (also see sidebar). These systems are designed to supplement the coverage from NEXRAD in and around the Bay Area and increase the accuracy of quantitative precipitation estimation (QPE). The use of smaller radar systems to fill gaps in the NEXRAD network supports recommendations for priorities in NOAA weather research (NOAA Science Advisory Board 2021). The QPE derived from AQPI radars has been shown to have better accuracy and improve streamflow simulations compared to NEXRAD (Cifelli et al. 2018; Ma et al. 2021).

Importantly, the AQPI radars can detect narrow cold-frontal rainbands (NCFRs) in parts of the Bay Area that are not well observed by NEXRAD (Fig. 3). NCFRs are rainbands that often occur along the cold-frontal boundary of extratropical cyclones that can produce high-intensity rain rates (Hobbs 1978) and are often responsible for flash floods and geomorphic hazards such as debris flows (Collins et al. 2020; de Orla Barile et al. 2022).

To date, two X bands have been installed and are operating as shown in Fig. 2. The characteristics of these radar units are described in Cifelli et al. (2018). The pandemic, wildfires, and power outages have delayed the installation of two X-band radars and the C-band radar which are expected to be installed by 2023.

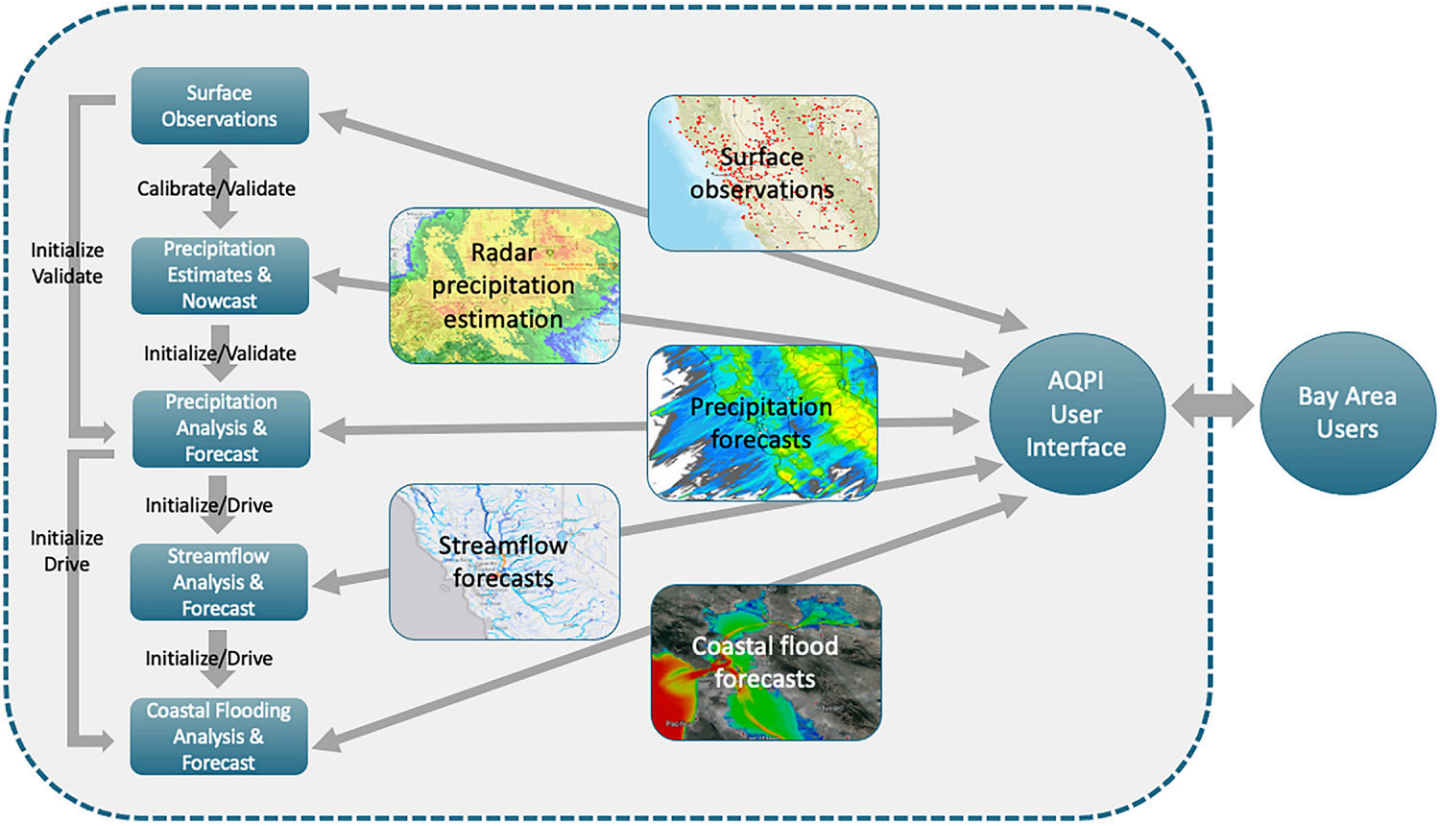

Fig. 1. Components of AQPI and the flow of information to and from the AQPI system user interface and Bay Area users.

Additional observations include preexisting station network data that are widely available [e.g., Hydrometeorological Automated Data System (HADS); Kim et al. 2009], new surface meteorological and precipitation profiling radar stations installed by NOAA/PSL for AQPI and another statewide observing project supported by CA DWR (White et al. 2013), as well as station data from existing local networks that were previously only available to individual water agencies. All of the station data are brought in through the NOAA Meteorological Assimilation Data Ingest System (MADIS; https://madis.ncep.noaa.gov/; Miller et al. 2005), taking advantage of the MADIS integration and QC capabilities to provide data standards for all datasets.

In addition to observations, forecast models are used to make predictions of precipitation, streamflow, and coastal flooding in the AQPI region. The domain of model coverage is shown in Fig. 4.

Description of AQPI forecast modeling

AQPI utilizes and couples several modeling systems to provide forecasts of precipitation, streamflow, and water levels in and around the Bay coastline. Here, we provide a brief description of each modeling component.

High-Resolution Rapid Refresh and Global Forecast System. High-Resolution Rapid Refresh (HRRR) is a numerical weather prediction model run operationally at the NOAA National Centers for Environmental Prediction (NCEP) and widely utilized by the NWS over the conterminous United States and Alaska. The HRRR is designed for optimal short-term forecasts, with an emphasis on capturing the evolution of precipitating systems. Its horizontal grid spacing is 3 km, and thus is a convection permitting modeling system. It is initialized hourly, assimilating a wide range of observations including Multi-Radar Multi-Sensor (MRMS; Zhang et al. 2016) radar reflectivity, radiosonde and aircraft thermodynamic and

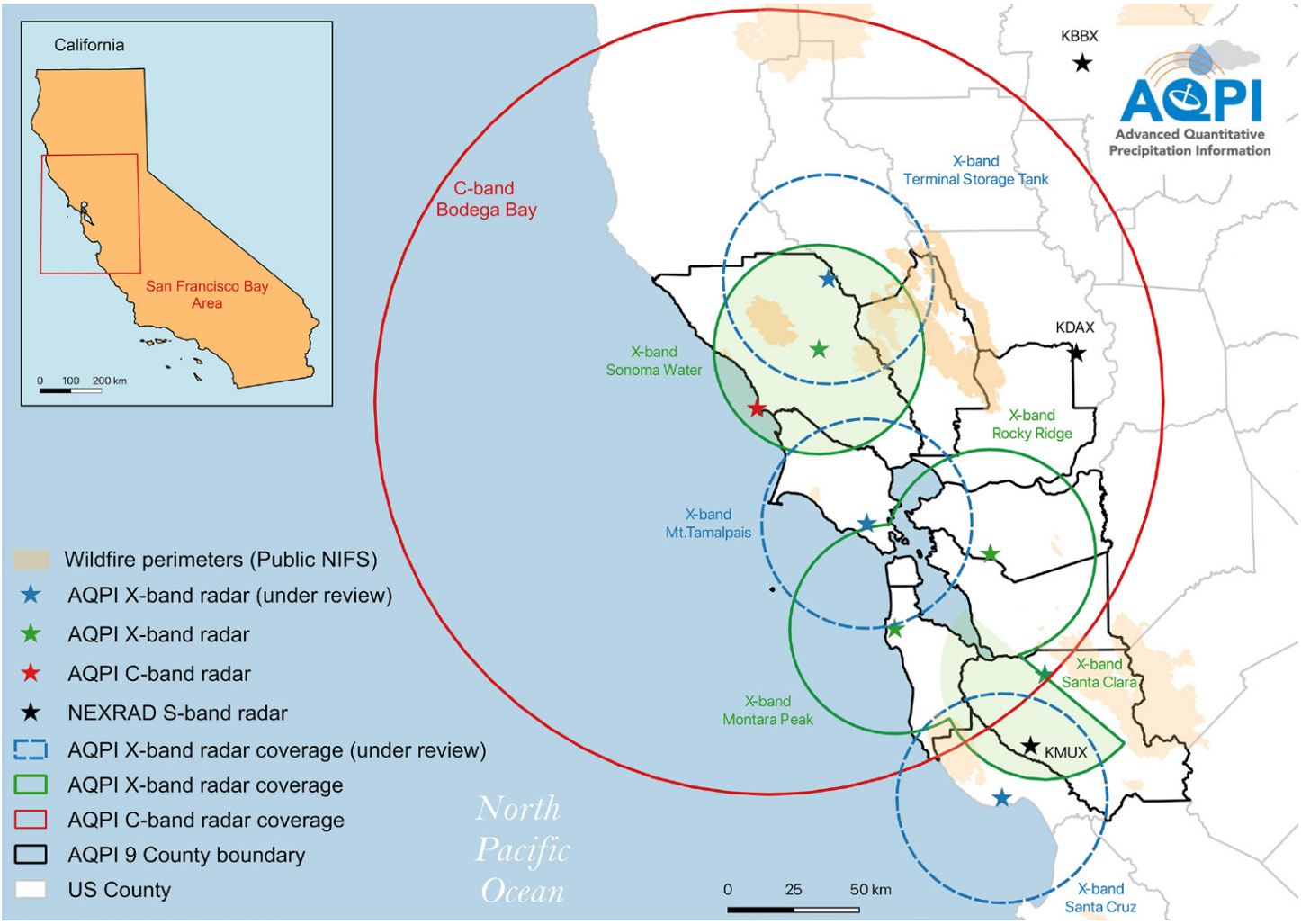

Fig. 2. Location of the radar network for AQPI. X-band systems supported by CA DWR are shown in green with the circles indicating a 40-km range of coverage. To date, the Sonoma and Santa Clara X bands have been installed and are operational (indicated with shading). The proposed C-band location is shown in red with the circle indicating 100-km range for rainfall analysis. The blue dashed lines indicate additional X-band systems that have been supported by other funding agencies and will be integrated into AQPI when they come online.

wind profiles, surface meteorological terminal air report (METAR) observations, cloud information from ground-based ceilometers and satellite observations, and more. MADIS serves as the conduit for acquiring many of these observations. As a regional model, the HRRR gets its boundary conditions from the 13-km Rapid Refresh (RAP) model (Benjamin et al. 2016), which uses the same dynamic core and physical parameterizations as the HRRR (except that convection is parameterized in the RAP). NOAA's Global Systems Laboratory (GSL), working with other partners such as the NWS Environmental Modeling Center (EMC), are continually improving the model's physical parameterizations and data assimilation system. The HRRR first became operational in 2014, with subsequent updates in 2016 (version 2), 2018 (version 3), and 2020 (version 4). Importantly, version 3 provided 36-h forecasts when initialized at 0000, 0600, 1200, and 1800 UTC; version 4 now provides 48-h forecasts at those times (the forecast length for other initialization times is 18 h). A full description of the model setup, physical parameterizations, and changes between the model versions is provided by Dowell et al. (2022) and James et al. (2022). As part of the AQPI project, the ability of the HRRR to forecast precipitation during AR events was assessed, which demonstrated that both version 3 and version 4 were able to capture these events well relative to observations, although the HRRR was somewhat dry biased in the Central Valley and moist biased in the Sierra Nevada (English et al. 2021).

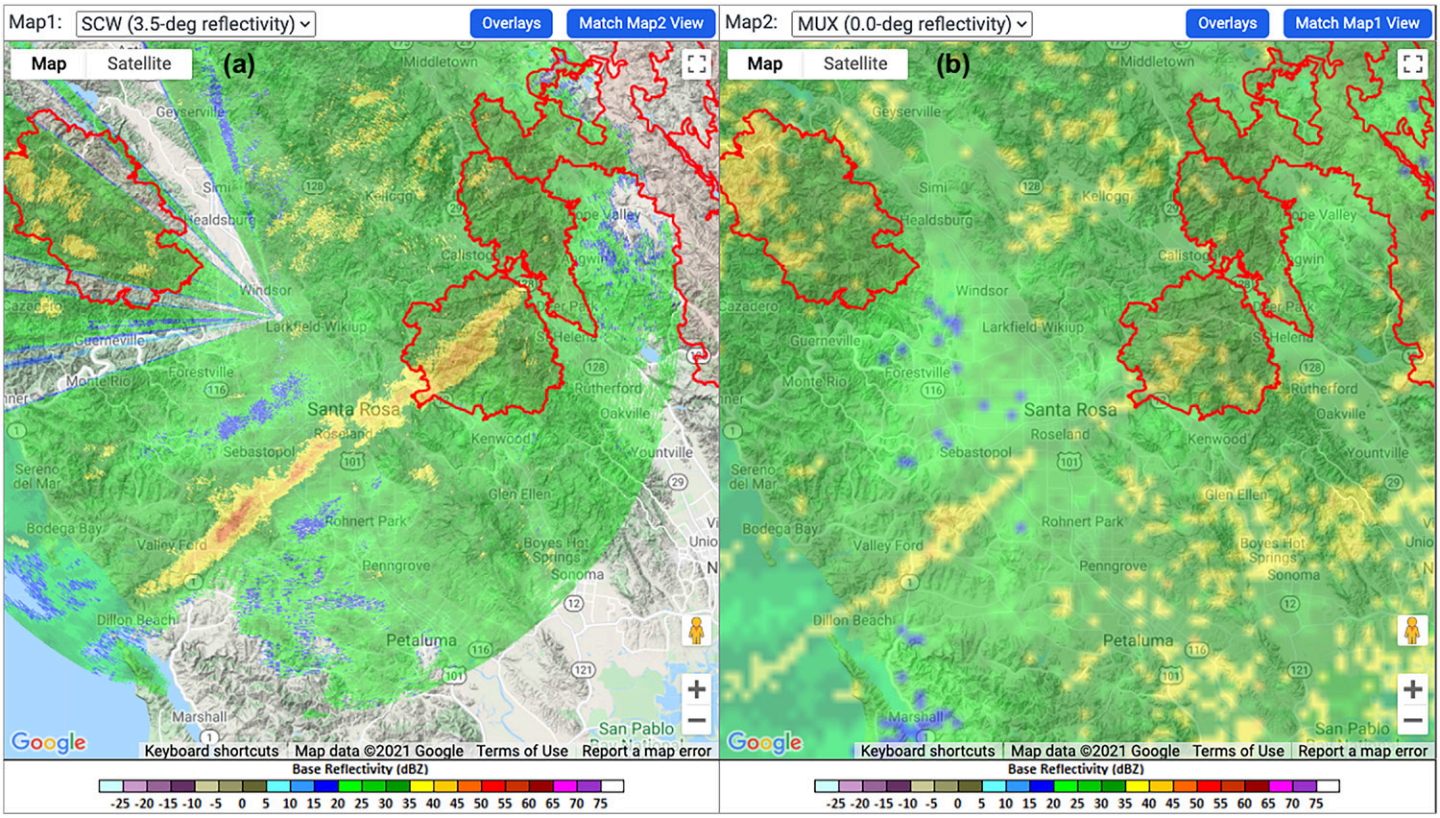

Fig. 3. Comparison of radar reflectivity from (a) AQPI X band and (b) KMUX NEXRAD during an AR event observed at 1846 UTC 24 Oct 2021. The narrow ribbon of high radar reflectivity near Santa Rosa in the center of each image represents a NCFR. Areas outlined in red represent recent burn scars.

The Global Forecast System (GFS) is the NWS's operational medium-range global forecast model. It is initialized 4 times per day at 0000, 0600, 1200, and 1800 UTC, generating forecasts out to 16 days. Its horizontal grid spacing is 13 km. It is initialized with a wide range of satellite, ground-based, and airborne observations using a three-dimensional variational data assimilation system. In 2019, its dynamic core was upgraded from a global spectral model framework to the finite-volume cubed sphere (FV3) as part of the Unified Forecast System (UFS; Jacobs 2021) effort, and at the same time the number of vertical levels was increased from 64 to 127. Like the HRRR, the physical parameterizations within the GFS are continually being updated by the NWS EMC and partners, with regular updates propagated to operational status in NWS. Details on the model, including its evolution over time, can be found on the NWS GFS website (www.emc.ncep.noaa.gov/emc/pages/numerical_forecast_systems/gfs.php).

NWM. The National Water Model (NWM) is a relatively new hydrologic modeling system developed by NOAA's Office of Water Prediction and the National Center for Atmospheric Research (NCAR). The NWM is based on the open source WRF-Hydro modeling framework developed by NCAR (Gochis et al. 2021). Details of the model's configuration are available from the Office of Water Prediction's website (https://water.noaa.gov/about/nwm). Briefly, the NWM simulates current and future streamflow at approximately 2.7 million stream reaches across the conterminous United States as well as Hawaii, the Virgin Islands, and Puerto Rico on a 1-km grid. This includes over 11,000 stream reaches in the AQPI domain. The NWM uses the Noah-MP (Niu et al. 2011) land surface model to simulate surface processes. Surface water routing is performed on a 250-m grid using a diffusive wave scheme and Muskingum–Cunge channel routing. The NWM is run in different analysis and forecast configurations for short- (18-h), medium- (~10-day), and long-range (30-day) hydrologic predictions. For the purposes of AQPI, the standard analysis and assimilation (current conditions)

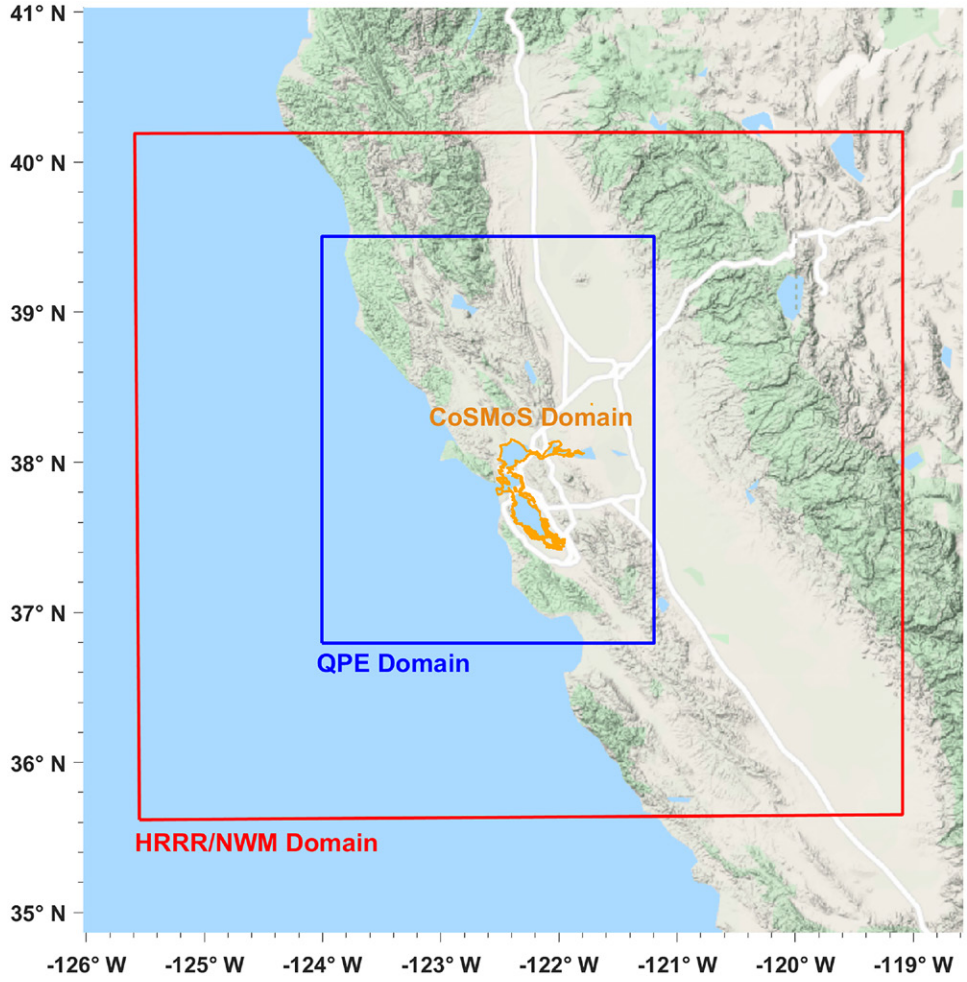

Fig. 4. Domain of coverage for modeling components of AQPI: HRRR/NWM, QPE, and CoSMoS domains are shown in red, blue, and orange, respectively.

and short-term forecast (18-h) configurations are most relevant since these use gauge and radar observations as well as HRRR model data to force the NWM. These configurations, as well as most of the others used by the NWM, benefit from the assimilation of USGS and U.S. Army Corps of Engineer hourly streamflow data as well as the inclusion of reservoirs and River Forecast Center forecasts of reservoir outflows at some locations. The analysis and short-term forecast configurations are cycled hourly.

Kim et al. (2021, manuscript submitted to *J. Hydrol.*) evaluated the performance of the short-range configuration of the NWM (v1.2) during the 2018/19 wet season. The analysis used 65 USGS stream gauges in the San Francisco Bay Area and showed that, based on Nash–Sutcliffe efficiency (NSE), the NWM provided useful forecasts (i.e., NSE > 0) out to about 10 h of forecast lead time. However, significant variation in forecast skill was observed in high flow versus low flow and natural versus managed river systems. The best overall skill was found in high-flow, natural watersheds.

CoSMoS. The USGS Hydrodynamic Coastal Storm Modeling System (Hydro-CoSMoS; hereafter referred to as CoSMoS; Tehranirad et al. 2020) applied in this system is based on the 1D–2D Still Water Level San Francisco Bay Community model (d3d-baydelta.org; Nederhoff et al. 2021). CoSMoS is an operational application of the Community model, the ocean boundary is forced with astronomical tides and forecast sea surface anomalies from the Global Water Level Forecast System (HYCOM; Chassignet et al. 2007). The tributaries are forced with the discharges provided by the nearest stream segment in the NWM. The surface boundary of the model is forced by surface mean sea level pressure, surface wind velocities, and precipitation

fields forecast by the HRRR model. Additionally, a wave model (SWAN; Booij et al. 1997) is run with the same atmospheric inputs. The offshore swell forecasts at the oceanic boundary are provided by the global WAVEWATCH III forecasts from NCEP (https://polar.ncep.noaa.gov/waves/wavewatch/). It provides 19-h forecasts of water level and/or depth and wave parameters from these two models, including significant wave height, direction, and period.

CoSMoS shows great skill in reproducing water levels in a hindcast mode using observations as inputs. Nederhoff et al. (2021) reported an average of 8-cm root-mean-square error (RMSE) over a 70-yr retrospective analysis. In most of the coastal areas of the bay, the highest water levels are driven primarily by the tides and offshore sea level anomalies. However, in the vicinity of rivers and other tributaries within the bay, the fluvial discharges can play an important role in driving high water levels. Tehranirad et al. (2020) showed that during February 2019, discharges contributed up to 5–10-cm surge in water levels in the North Bay, highlighting the role of accurate discharges in projecting how much area will be inundated. In a case study of water levels in San Mateo Creek (one of the smaller managed drainages into San Francisco Bay), in the region where both discharges and tides are important to total water level, the forecast is more sensitive to the magnitudes of discharge than to predicting the timing correctly. When accounting for potential phasing issues by comparing daily forecast peaks to observed daily peaks, the error is approximately half that observed by the time matched errors (7- versus 14-cm RMSE). Overall, the baywide water levels are highly accurate. Although the exact timing of peak water levels is more likely to be shifted near fluvial discharges, the daily forecast peak will still be near the observation.

AQPI system

The AQPI team determined that a single data access system was needed to provide "one-stop shopping" that could serve the needs for all of the stakeholders in the Bay Area region. The AQPI system integrates all the observation and model data and provides it in usable formats with customized threshold alerts for decision-making purposes. From the beginning, the system was designed with significant input from local water management agencies to determine needs and requirements for precipitation, streamflow, and coastal flooding information. The AQPI research team conducted a number of in-person meetings with Bay Area water agency representatives to identify specific geographic areas of concern and desired thresholds for rainfall, streamflow, and/or coastal water levels to take action in advance and during a flooding event. Because the water agencies can have somewhat different missions (flood protection, wastewater, water supply, etc.) and encompass regions with differing characteristics (land use, terrain, proximity to the Bay, etc.) the needs and requirements vary with each agency. These meetings resulted in an extensive list of needs and requirements, which were used to build the AQPI system. One example is the San Francisco Public Utilities (SFPUC), which is concerned with potential flooding impacts of water releases from Lower Crystal Springs Reservoir on San Mateo Creek, especially near Highway 101 where the creek meets the Bay. Forecasts of Bay water levels from CoSMoS will help inform SFPUC's decision-making concerning outflows from the reservoir (A. Dufour, SFPUC, 2021, personal communication).

As noted above, one of the drivers for the AQPI system is to consolidate desired information on precipitation, streamflow, and coastal water levels in the Bay Area. To this end, MADIS is used to collect and distribute data in the AQPI domain. An additional advantage of adding local data is that the precipitation information available in MADIS is used to bias correct MRMS QPE products and improve their overall skill. To date, 295 local network stations have been added through MADIS and the AQPI system is providing data and services (described below) to 13 water agencies in the Bay Area.

Model forecast data from the HRRR, GFS, NWM, and CoSMoS are made available to users for their specific domains of interest. This information can be used independently for situational

awareness or used to drive other "local" models. For example, in Santa Clara County, the radar data are used for real-time storm monitoring to inform potential areas of flooding concern (J. Xu, Valley Water, 2021, personal communication). In Contra Costa County, NWM data are used as input to a Hydrologic Engineering Center River Analysis System (HEC-RAS) model to inform on flows in areas of concern. As another example, the SFPUC Wastewater enterprise is using the AQPI HRRR forecasts to predict 18-h rainfall accumulation across different quadrants of the city as well as to identify short duration periods (1 h) with predicted rainfall rates exceeding flood return period criteria. The goal is to eventually bring the information down to the neighborhood scale to better identify parts of the city that may be at flood risk during a rain event (M. Chokshi, SFPUC, 2019, personal communication).

AQPI radar data are used to generate QPE and "nowcast" products and is also sent to the National Severe Storms Laboratory and integrated with NEXRAD data in the development version of the MRMS product. Future efforts are aimed at transitioning the AQPI data into the operational version of MRMS so that it can be assimilated by the operational HRRR model.

The AQPI graphical user interface is designed to display real-time model and observational data to users and is customized for each water agency. Users can select products of interest for their geographic regions of concern and preset thresholds for precipitation, streamflow, and coastal flooding. Users can view and download the AQPI observation and model data updated in real time.

AQPI products

AQPI includes a number of products from both the observations and models as shown in Table 2. Some products are simply model forecasts of precipitation, streamflow, and coastal water levels from the modeling systems described above, customized for the water agency's region of interest. Other products are derived from observations. This includes QPE and nowcast. The QPE product includes a blend of AQPI radar data where the X bands provide coverage and MRMS data to cover the rest of the domain. The AQPI radar QPE builds on the specific differential phase approach described in Cifelli et al. (2018) and Biswas et al. (2020). The current version of the QPE is based on the application of optimum radar rainfall estimators (both reflectivity and specific differential phase based), which is guided by an orographic/stratiform rainfall type classification as discussed in Biswas et al. (2024). It also includes an algorithm to mitigate brightband contamination. The MRMS radar-only QPE is used to fill the QPE in the remainder of the AQPI domain outside the coverage of the AQPI radars as well as areas within the AQPI radar coverage domain that are blocked by terrain or other features. Both 15-min and hourly QPE are provided with an update time of 2 min. An example of the QPE product is shown in Fig. 5.

Table 2. Description of AQPI products.

AQPI product	Inputs	Description
Precipitation and near-surface temperature forecasts	HRRR+GFS	Hourly forecast out to 18 h updated each hour with HRRR; GFS forecast appended to end of each 18-h HRRR forecast out to 120 h at 3-h intervals to 90- and 6-h intervals from 90 to 120 h; GFS updated every 6 h
Streamflow forecasts	NWM	Hourly forecast out to 18 h updated each hour
Coastal water level forecasts	CoSMoS	Hourly forecast out to 18 h using latest HRRR forecast and using latest NWM forecast
QPE	AQPI+MRMS radar-only QPE	15- and 60-min rainfall accumulation updated every 2 min
Nowcast	MRMS radar-only QPE	Precipitation nowcast out to 60 min updated every 2 min

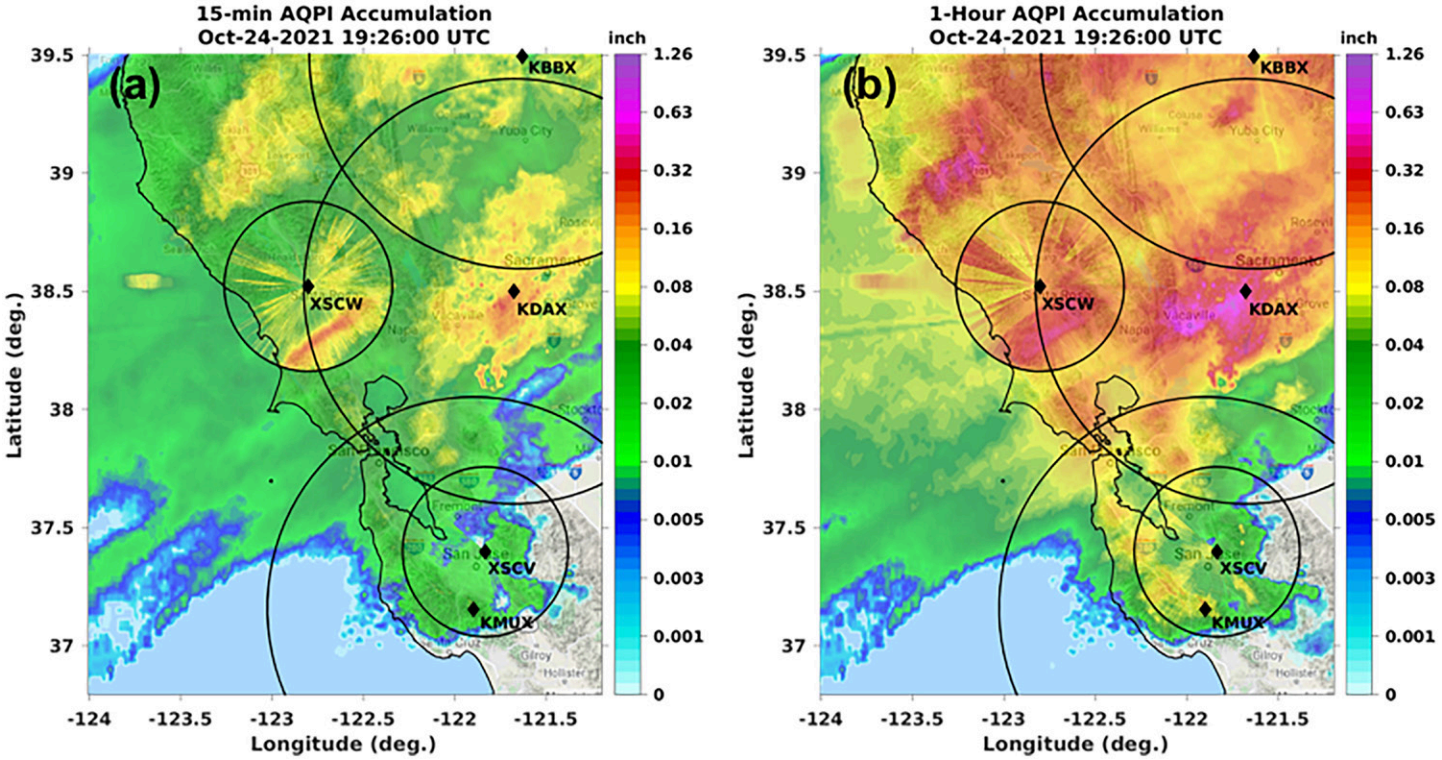

Fig. 5. (a) 15-min and (b) hourly QPE ending at 1926 UTC 24 Oct 2021. The QPE map is constructed using a combination of AQPI radar QPE within the small circles and MRMS radar-only QPE over the rest of the domain. Small circles show the 40-km range rings of AQPI X-band radars located near Santa Rosa (XSCW) and Santa Clara (XSCV) and the larger circles represent the 100-km range ring of the NEXRAD KMUX and KDAX radar systems. Note that the streaks in the XSCW circle represent terrain blockage.

Note the "spike" appearance in QPE, especially in the northern part of the XSCW domain. This pattern indicates blockage of the AQPI radar signal resulting from objects near the radar site. MRMS data are currently used to fill gaps, which is less than ideal given the challenges with NEXRAD coverage in this area. There are long-term plans to raise the XSCW radar to help reduce the blockage or move it to an alternate location.

The AQPI real-time nowcast system uses the Dynamic and Adaptive Radar Tracking of Storms (DARTS; Ruzanski et al. 2011) nowcast tool to extrapolate radar observations of precipitation (QPE) for the next 60 min. DARTS is an area-based nowcast tool, and it solves the field flow equation in the frequency domain. A fast Fourier transform (FFT) technique is used for fast computation. Currently, the AQPI real-time nowcast uses the MRMS radar-only QPE product to generate the nowcast. In the future, a blend of AQPI and NEXRAD data will be used.

In addition to CoSMoS-derived water level forecasts in the Bay, AQPI includes displays of coastal flood inundation from CoSMoS. These outputs include the water level referenced to NAVD88, the water depth referenced to a recent DEM (Danielson et al. 2016) and wave parameters. The wave fields include wave height, period, and direction and can be used to assess the risk of wave-driven overtopping of nearby levies or sea walls. Additionally, depth-averaged currents can be obtained from the outputs, although those are not available as graphic displays. The CoSMoS information can be used to help assess risks for overtopping coastal defenses such as levees and sea walls and timing of freshwater releases that will not be blocked by high coastal water levels.

AQPI benefits

AQPI was designed to support a number of water management activities across the Bay Area. While AQPI does not give a sufficiently long-range forecast for large reservoir operations, it

could help managers of smaller reservoirs time appropriate discharges before and during heavy rain events in order to maintain water supplies and not exacerbate flood damage downstream. Wastewater treatment plant operators around the Bay would be able to take remedial actions when these events include a significant storm surge. As described below, another benefit is that flood protection agency managers would be able to better anticipate flooding events and thus more effectively deploy their assets to deal with them.

Johnson et al. (2020) conducted a reconnaissance-level overview of potential benefits of the AQPI system, examining the impact to different economic sectors including flood damage mitigation, increasing water supplies, and enhancement of ecological, recreational, and transportation services with the highest benefit (48%) associated with avoided flood damages. Benefit to costs were estimated to range of 2:1 to 10:1 with the most likely being 5:1. The large range reflects the uncertainty in the percentage of water management agencies and citizens that take appropriate action, emphasizing the importance of outreach and training to maximize responses.

Current economic impact studies are underway with individual water management agencies to better quantify benefits of AQPI information across the Bay Area. In particular, members of the project team have integrated the AQPI system with hydrologic, civil engineering, and economic impact models built specifically for Santa Clara County that allow estimating the potential economic benefits arising from better and more advanced flood predictions. The economic benefits focus on changes in employment, real household income, and sector level gross domestic output. The basic intuition is that more timely, spatially defined warnings can allow local governments, businesses, and homeowners the additional time needed to implement short-term mitigation strategies that can help reduce direct financial and subsequent economic losses. We compare two simulations: 1) estimating the economic losses of a simulated flood due to the damage to commercial and residential buildings, and 2) estimating the impacts of the same flood when short-term mitigation strategies are implemented (e.g., sandbagging, installing short-term pumps, moving contents to a second floor). The reduction in economic losses from the two simulations will represent the value of the AQPI system and will be the focus of a future journal publication.[2]

[2] Previously, computable general equilibrium (CGE) models have been constructed to estimate the economic impact of evaluating improvements in NOAA's HRRR system for forecasting precipitation, wind, and temperature. As examples, see Hartman et al. (2021), Turner et al. (2022), and Jeon et al. (2022).

Preliminary results

To demonstrate the value of the AQPI approach, we use an event from 27 to 28 January 2021 to illustrate the system functionality and components. An overview of the event is provided by the Monterey Forecast Office (www.weather.gov/mtr/AtmosphericRiver_1_26-29_2021). The event was the biggest storm of the 2020/21 water year in the Bay Area with 2–4 in. (~5–10-cm) precipitation accumulations in the urban regions and much higher accumulations farther south (10–15 in.; 25–38 cm) in the Santa Lucia Mountains. Based on the duration and integrated water vapor transport characteristics, the event was probably an AR2 using the scale developed by Ralph et al. (2019). According to the Ralph et al. study, AR2 events are described as being "mostly beneficial but also hazardous." Although similar in many respects to ARs impacting central California during the winter season, it was a "cold" event with low freezing levels and produced snow on the peaks surrounding the Bay Area (Fig. 6). The Weather Prediction Center issued high risk for flooding on both 27 and 28 January and flash flood warnings were issued for many of the burn scar regions in the area with resulting debris flows occurring in some parts of Central and Southern California.

The performance of the operational NOAA HRRR precipitation forecast for the period extending from 0000 UTC 27 January to 1200 UTC 29 January is shown in Fig. 7. In particular, the 6-h precipitation accumulation forecast was evaluated. Overall, the HRRR performed quite

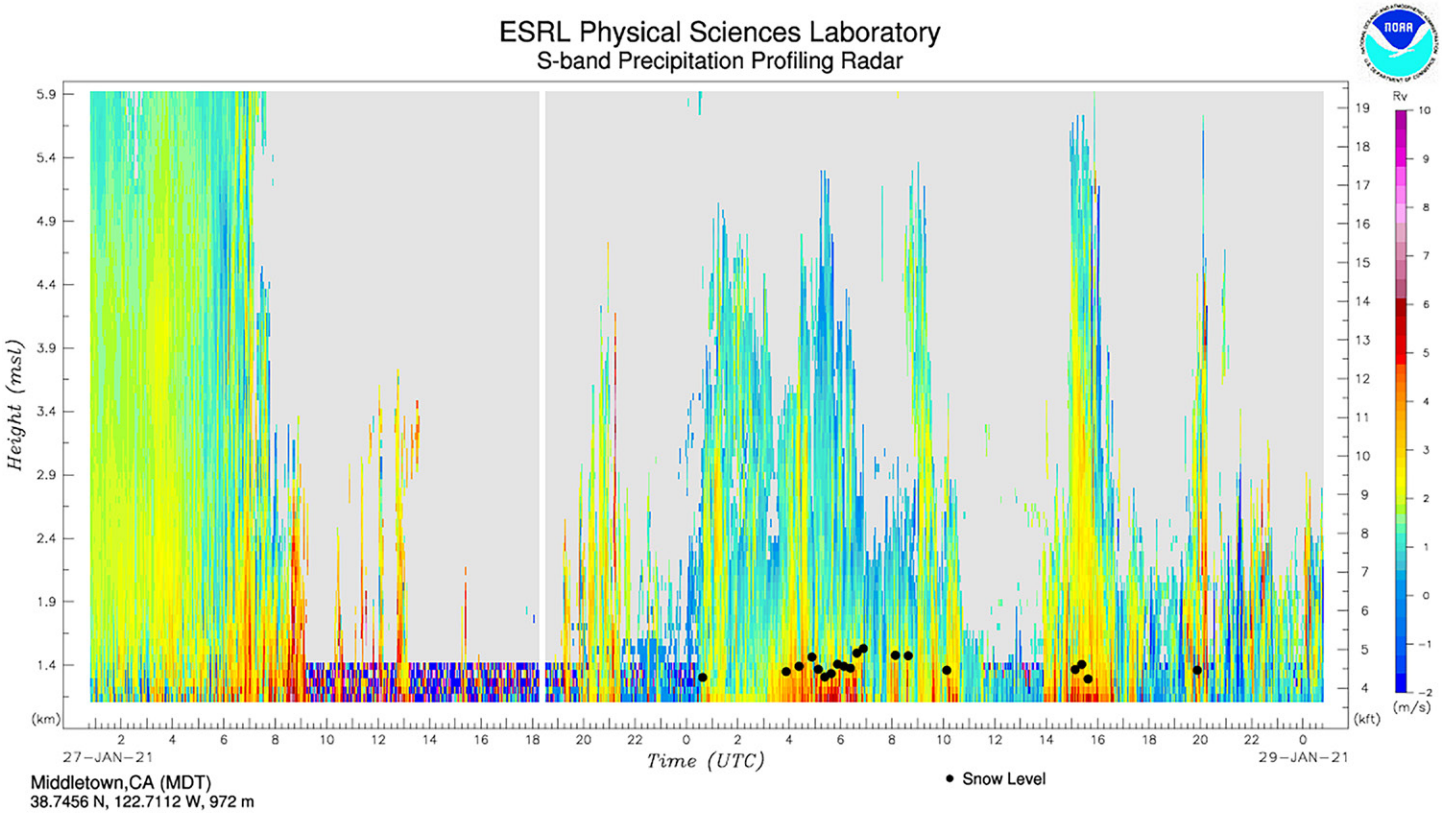

Time (UTC)	0115	0215	0315	0415	0515	0615	0715	0815	0915	1015	1115	1215	1315	1415	1515	1615	1715	1815	1915	2015	2115	2215	2315	0015
Snow Level (m)	none	none	none	none	none	none	none	none	none	none	none	none	none	none	none	none	none	none	none	none	none	none	none	1303
Snow Level (ft)	none	none	none	none	none	none	none	none	none	none	none	none	none	none	none	none	none	none	none	none	none	none	none	4273
Sfc Temp (C)	−0.69	−0.66	−0.67	−0.23	0.06	0.30	0.43	1.29	1.41	1.95	2.37	2.32	2.21	1.77	1.65	2.03	2.35	2.46	3.09	2.95	3.00	3.14	2.85	2.90

Time (UTC)	0115	0215	0315	0415	0515	0615	0715	0815	0915	1015	1115	1215	1315	1415	1515	1615	1715	1815	1915	2015	2115	2215	2315	0015
Snow Level (m)	none	none	none	1370	1350	1399	1531	1476	none	1360	none	none	none	none	1366	none	none	none	none	1360	none	none	none	none
Snow Level (ft)	none	none	none	4493	4428	4590	5021	4841	none	4460	none	none	none	none	4480	none	none	none	none	4460	none	none	none	none
Sfc Temp (C)	2.41	2.05	1.65	1.54	1.57	1.61	2.77	3.22	3.42	3.26	3.28	3.11	3.15	3.29	3.22	2.78	3.02	3.32	3.36	3.31	3.45	3.54	3.68	3.48

Fig. 6. The snow-level display produced from data collected by an S-band precipitation profiling radar located in Middletown, California, at 972-m elevation. Colors represent the Doppler vertical velocity (m s^{-1}; color scale on right), which is dominated by hydrometeor fall velocity in precipitation. The table lists the snow level (when it is above the radar) and the surface temperature. Precipitation fell as snow on 27 Jan, before transitioning to a cold rain on 28 Jan with snow levels remaining below ~1.5 km MSL. This profiling radar was installed prior to AQPI with support from the Sonoma Water Agency and is being leveraged as part of the AQPI project.

well during this event, but had a dry bias along the Pacific coast and a wet bias in the Sierra range similar to other cases evaluated in English et al. (2021).

A detailed evaluation of the AQPI radar QPE was conducted for this event as described in Biswas et al. (2024). Scatterplots and error statistics for both of the operating AQPI radars are shown in Fig. 8. The AQPI radar QPEs showed good skill overall with improvement over both the MRMS QPE products in terms of bias, error, and correlation statistics. While not as good as the Santa Clara radar performance, the Sonoma radar QPE shown in Fig. 8 is still a large improvement over MRMS QPE. Differences in performance between the two radars are likely a result of the more complicated terrain surrounding the Sonoma versus the Santa Clara radar. Also, as discussed in Biswas et al. (2024), there is a lot of QPE performance variability from event to event, depending on the height of the melting layer and the amount of orographic enhancement resulting in variability of raindrop size distribution. However, in all cases examined, the AQPI radar QPE product outperforms both MRMS radar-only and Multisensor Pass1 QPE products. Future efforts to improve the AQPI QPE will include implementing a composite QPE product that will combine information from higher-elevation radar scans to fill in the gaps. Additionally, efforts are being made to examine possible machine learning approaches that will use ground-based rain gauge data for QPE correction.

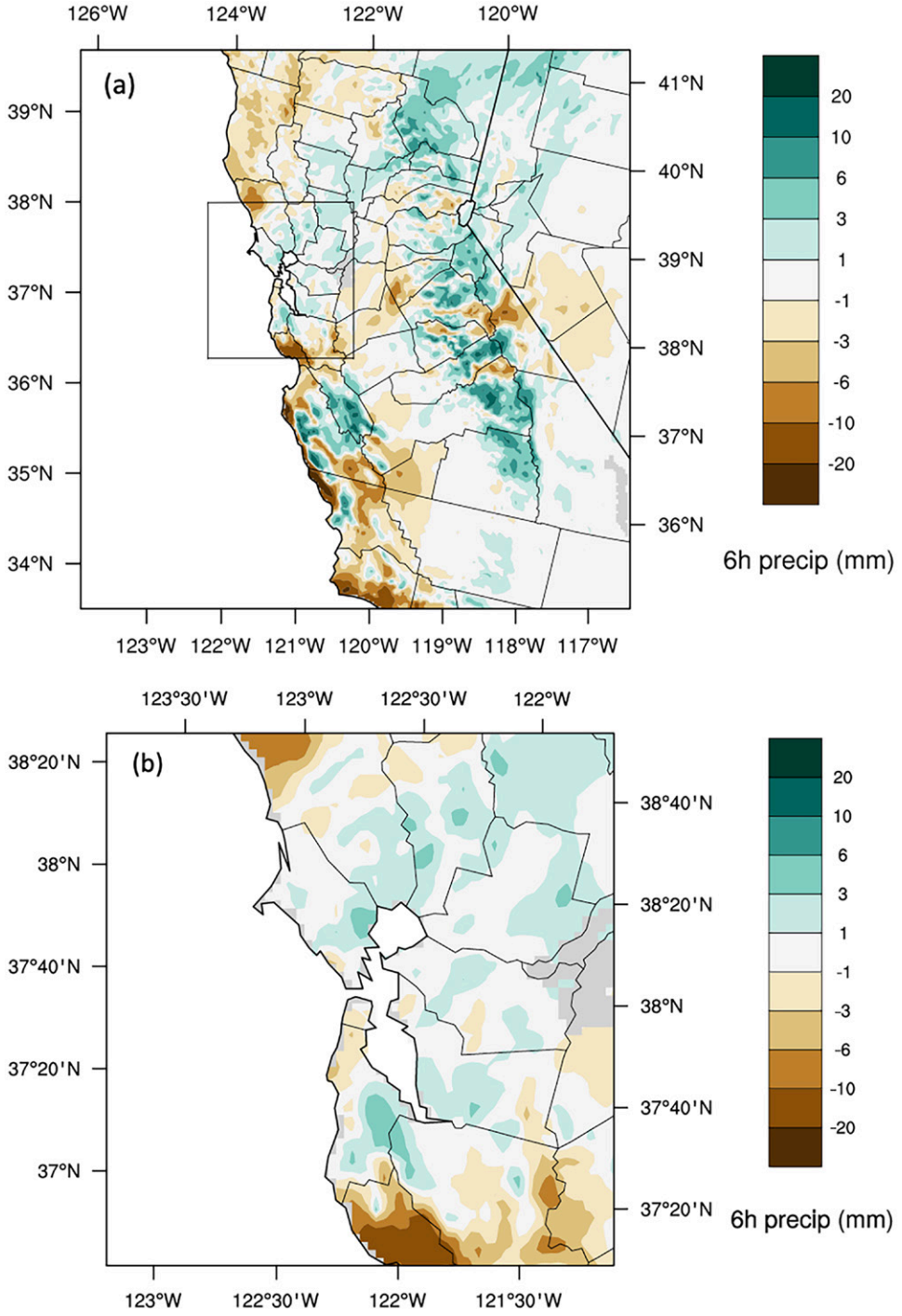

Fig. 7. Difference plot of all HRRR 6-h precipitation accumulation (6-h forecasts) and associated stage IV QPEs for the period 0000 UTC 27 Jan to 1200 UTC 29 Jan 2021. (a) Full AQPI domain with Bay Area outline indicated by black rectangle. (b) As in (a), but for Bay Area region only. Warm colors indicate an underestimate of HRRR precipitation relative to stage IV while cool colors indicate an overestimate.

As shown in Fig. 9, the NWM 18-h forecasts were evaluated from 0000 UTC 27 January to 2300 UTC 28 January 2021. The metrics used in the evaluation include Klein–Gupta efficiency (KGE; Gupta et al. 2009), NSE (Nash and Sutcliffe 1970), correlation coefficient (CORR), and RMSE, where NSE and KGE are commonly used statistics to calibrate and measure the predictive skill of hydrologic models. The results show the best performance at the shortest lead times, with errors rapidly decreasing until approximately 9-h lead time. These results are similar to Kim et al. (2021, manuscript submitted to *J. Hydrol.*) described above.

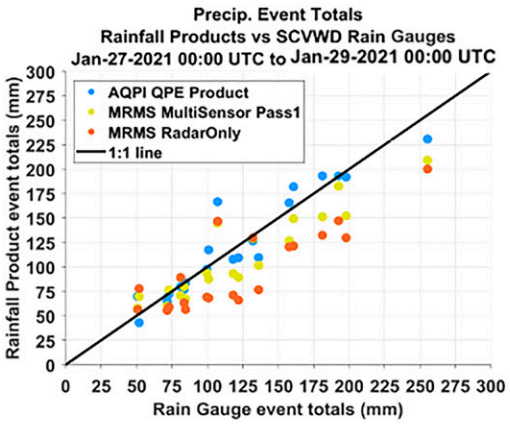

(a)

	Mean Bias (mm)	Mean Absolute Error (mm)	Root Mean Squared Error (mm)	Correlation
AQPI QPE Product	2.53	14.15	20.04	0.9
MRMS MultiSensor Pass1	-13.38	19.91	24.30	0.9
MRMS RadarOnly	-25.88	34.07	39.05	0.82

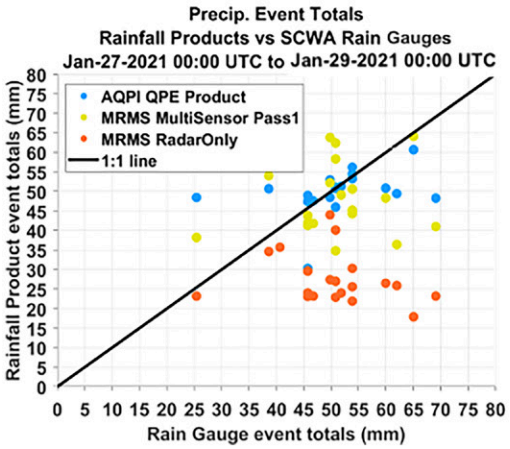

(b)

	Mean Bias (mm)	Mean Absolute Error (mm)	Root Mean Squared Error (mm)	Correlation
AQPI QPE Product	-0.17	6.78	10.00	0.35
MRMS MultiSensor Pass1	-1.78	10.37	13.00	0.1
MRMS RadarOnly	-22.78	22.00	26.20	-0.23

Fig. 8. Scatterplots and error statistics for the (a) Santa Clara and (b) Sonoma AQPI radar domains (blue) for the period from 0000 UTC 28 Jan to 0000 UTC 29 Jan 2021. Blue, yellow, and orange colors represent AQPI radar QPE, MRMS Multisensor Pass1, and MRMS radar-only, respectively.

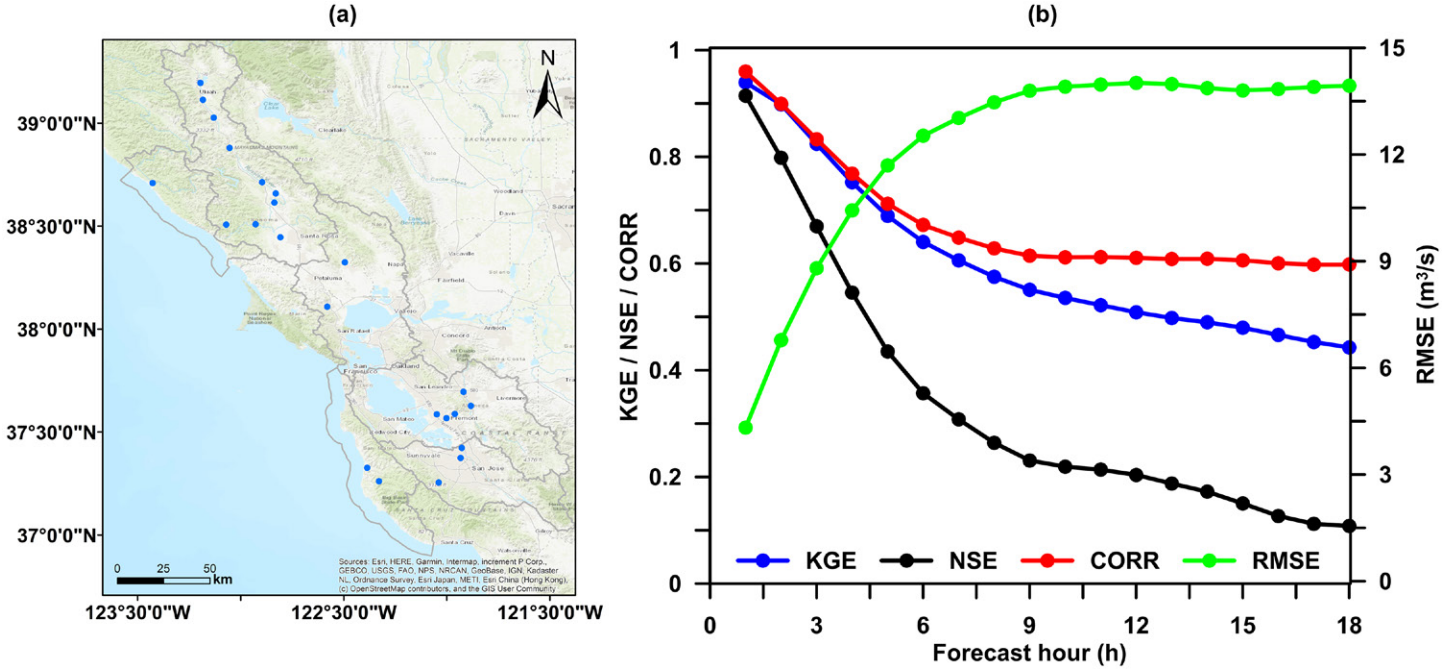

Fig. 9. Performance of NWM (V2.1) short-range forecast (1–18-h) streamflow products in the AQPI domain for the period from 0000 UTC 27 Jan to 2300 UTC 28 Jan 2021. (a) Location of USGS stream gauges (blue dots) used in this analysis, and (b) error statistics of NWM V2.1 short-range forecasts at the lead times of 1–18 h, including KGE (blue), NSE (black), CORR (red), and RMSE (green).

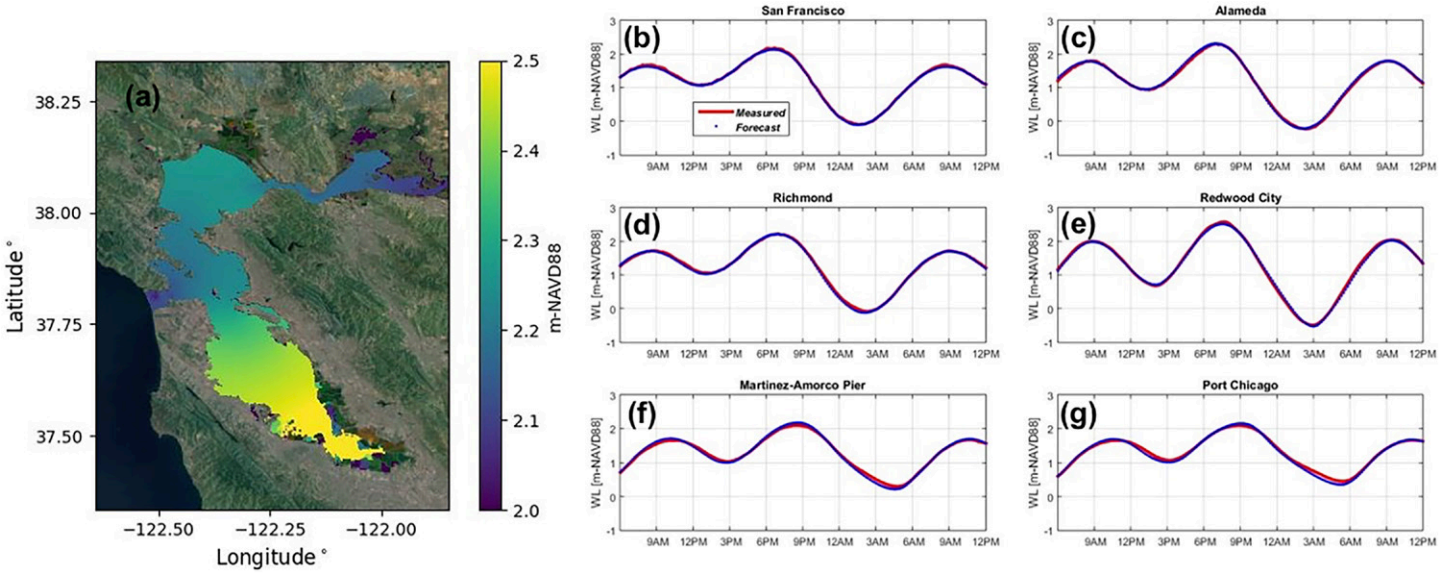

Fig. 10. Performance of Hydro-CoSMoS short-range forecast water-level products during the 27–28 Jan event. (a) Map of maximum water level in meters relative to NAVD88 over the 18-h forecast started on 0600 UTC 28 Jan. (b)–(g) Comparison of modeled and observed water levels at selected NOAA COOPS tides and currents stations.

An evaluation of the CoSMoS short-range forecast was also conducted for the 27–28 January event. As shown in Fig. 10, although no significant coastal flooding occurred during this event the water levels throughout the bay were predicted very well. The highest water level at the San Francisco station occurred just after 1800 LT 28 January. During this time period, the water levels were more than 20 cm above the tidally predicted values. The model error (mean bias) over this time period ranges from –2.48 cm (at Port Chicago) to 1.52 cm (at Alameda).

Next steps for AQPI

AQPI has advanced to the point that the information delivered by this system is being used by local water managers on a regular basis. The information will continue to improve as the additional radar systems come online, are integrated into the AQPI system providing improved nowcasted QPF products, and are assimilated into the operational HRRR and the HRRR's eventual replacement—the Rapid Refresh forecast system. Water agencies have already developed methods to integrate the information into their operations and this process is expected to accelerate over time. To facilitate this process, AQPI has developed a Data Implementation Working Group where local users from the water management community interact with the technical development team and provide ongoing feedback to improve the system's products and services as well as talk about ways to help each other use the AQPI information effectively and provide lessons learned. Still, challenges lay ahead for AQPI, including where the system will ultimately reside after NOAA completes development and hands it off, and how the annual operations and maintenance costs will be supported. Toward that end, AQPI has implemented a Local Partner Advisory Committee (LPAC) to help resolve issues related to radar and other instrument deployments, outreach for the program, and the development of a plan for long-term operations of AQPI data system.

The concept of AQPI, where improvements to high-resolution observations and forecasts are driven by end users working closely with scientists and developers to improve informed decision-making could be replicated in other urban centers in the United States and abroad. Moreover, in California where flooding events are almost entirely restricted to the cool season, AQPI is exploring the benefit of leveraging the radar assets to track wildfire emissions during the warm season (e.g., Zrnić et al. 2020), as well as monitoring for postfire debris

flow hazards (e.g., Jorgensen et al. 2011). More information about AQPI, as well as access to real-time information can be found at https://psl.noaa.gov/aqpi/.

Acknowledgments. Thank you to Kelly Mahoney at NOAA PSL and three anonymous reviewers for reviewing the manuscript and providing helpful suggestions. The AQPI project has been supported through a grant from CA DWR, as well as through internal funding by NOAA PSL and GSL. Any use of trade, firm, or product names is for descriptive purposes only and does not imply endorsement by the U.S. Government. There are a large number of people in addition to the coauthor list who have contributed to the success of AQPI, too many to include here. However, we especially recognize Barb Deluisi and Rich Lataitis of NOAA PSL, Theo Stein of NOAA Office of Communications, and Jack Xu, Alexis Dufour, and Roger Leventhal from Valley Water, SFPUC, and Marin County Public Works, respectively, for their support, feedback, enthusiasm, and ideas to advance AQPI. Sen Chiao and Dalton Behringer, both formally from San Jose State, provided disdrometer data and atmospheric modeling results from AR events. The authors are especially appreciative of all the input and support from local water agency representatives to help work through the permitting challenges associated with radar siting and to help us understand how AQPI can help them improve their operations. We would like to dedicate this article to Carl Morrison, who was instrumental in launching the AQPI project, but passed away suddenly in the middle of the program.

Data availability statement. Datasets that are part of the AQPI system are available from the following sites online. Atmospheric model (HRRR and GFS) and National Water Model data are available through NOAA National Centers for Environmental Prediction (NCEP) website: www.nco.ncep.noaa.gov/pmb/products/. Surface data are available through the MADIS interface: https://madis.ncep.noaa.gov/ and the rough NOAA PSL at https://psl.noaa.gov/data/obs/datadisplay/. MRMS is also available at NCEP: https://mrms.ncep.noaa.gov/data/.

Weather radar frequency bands

Weather radars operate in different frequency bands. The most commonly used operational systems are at S band (2,700–3,000 MHz), C band (5,600–5,700 MHz), and X band (9,300–9,500 MHz). To first order, the minimum antenna size of the radar is inversely proportional to frequency, to support the narrow beams, which means radars operating at higher frequencies can have a smaller antenna size. This is an important consideration for overall cost and "agility" of the radar system. For example, S-band systems like WSR-88D have an antenna diameter of about 8.5 m. X-band systems like those used in AQPI are much smaller with an antenna diameter of about 1.8 m. They can be mounted in a variety of locations, including building rooftops and communication towers. C-band antenna diameters are in the range of 4.5m, making them less agile than X band but still transportable and a good compromise between S and X bands. For example, C-band radars have been deployed aboard research ships (see Rutledge et al. 2019).

Because of the enhanced cross section of meteorological targets with higher frequency, higher-frequency radar systems like X band can operate at lower power, and can provide the same sensitivity at moderate ranges. Higher-frequency electromagnetic waves experience attenuation due to propagation through rain. Even though techniques are available to correct for attenuation so long as there is a signal, the amount of additional power needed to mitigate attenuation effects is too high and it is cheaper to deploy another radar at a farther distance than to transmit extra power to mitigate attenuation. Therefore X-band radars are typically made for shorter ranges such as 40–60 km to be cost effective. Each of these frequency bands has certain advantages and are tailored for specific applications. S band and C band have been generally used to establish radar networks over large regions of continental scales. X-band networks are becoming the deployment of choice for urban areas as the social footprint of these radars are very low (e.g., transmitted power and radar size). The X-band systems can sit on existing infrastructure and, because of their relatively small size, they tend to be lower cost and can also be moved around easily (Chandrasekar et al. 2018). Often the infrastructure costs of weather radars far exceed the cost of radar itself in urban regions.

References

Benjamin, S. G., and Coauthors, 2016: A North American hourly assimilation and model forecast cycle: The Rapid Refresh. *Mon. Wea. Rev.*, **144**, 1669–1694, https://doi.org/10.1175/MWR-D-15-0242.1.

Biswas, S. K., R. Cifelli, and V. Chandrasekar, 2020: Improving quantitative precipitation estimation by X-band dual-polarization radars in complex terrain over the Bay Area in California, USA. *2020 IEEE Int. Geoscience and Remote Sensing Symp.*, Waikoloa, HI, IEEE, 5411–5414, https://doi.org/10.1109/IGARSS39084.2020.9323239.

——, ——, and ——, 2024: Quantitative precipitation estimation using X-band radar for orographic rainfall in the San Francisco Bay Area. *IEEE Trans. Geosci. Remote Sens.*, https://doi.org/10.1109/TGRS.2022.3207829, in press.

Booij, N., L. H. Holthuijsen, and R. C. Ris, 1997: The "SWAN" wave model for shallow water. *Coastal Engineering 1996*, Orlando, FL, Coastal Engineering Research Council, 668–676, https://doi.org/10.1061/9780784402429.053.

CA DWR, 2013: California's flood future: Recommendations for managing the state's flood risk. CA Department of Water Resources Rep., 152 pp.

Chandrasekar, V., H. Chen, and B. Philips, 2018: Principles of high-resolution radar network for hazard mitigation and disaster management in an urban environment. *J. Meteor. Soc. Japan*, **96A**, 119–139, https://doi.org/10.2151/jmsj.2018-015.

Chassignet, E. P., H. E. Hurlburt, O. M. Smedstad, G. R. Halliwell, P. J. Hogan, A. J. Wallcraft, R. Baraille, and R. Bleck, 2007: The HYCOM (Hybrid Coordinate Ocean Model) data assimilative system. *J. Mar. Syst.*, **65**, 60–83, https://doi.org/10.1016/j.jmarsys.2005.09.016.

Cifelli, R., V. Chandrasekar, H. Chen, and L. E. Johnson, 2018: High resolution radar quantitative precipitation estimation in the San Francisco Bay Area: Rainfall monitoring for the urban environment. *J. Meteor. Soc. Japan*, **96A**, 141–155, https://doi.org/10.2151/jmsj.2018-016.

Collins, B. D., N. S. Oakley, J. P. Perkins, A. E. East, S. C. Corbett, and B. J. Hatchett, 2020: Linking mesoscale meteorology with extreme landscape response: Effects of narrow cold frontal rainbands (NCFR). *J. Geophys. Res. Earth Surface*, **125**, e2020JF005675, https://doi.org/10.1029/2020JF005675.

Cordeira, J., J. Stock, M. Dettinger, A. Young, J. Kalansky, and F. M. Ralph, 2019: A 142-year climatology of Northern California landslides and atmospheric rivers. *Bull. Amer. Meteor. Soc.*, **100**, 1499–1509, https://doi.org/10.1175/BAMS-D-18-0158.1.

Corringham, T. W., F. M. Ralph, A. Gershunov, D. R. Cayan, and C. A. Talbot, 2019: Atmospheric rivers drive flood damages in the western United States. *Sci. Adv.*, **5**, eaax4631, https://doi.org/10.1126/sciadv.aax4631.

Crum, T., and R. Alberty, 1993: The WSR-88D and the WSR-88D Operational Support Facility. *Bull. Amer. Meteor. Soc.*, **74**, 1669–1687, https://doi.org/10.1175/1520-0477(1993)074<1669:TWATWO>2.0.CO;2.

Danielson, J. J., S. K. Poppenga, J. C. Brock, G. A. Evans, D. J. Tyler, D. B. Gesch, C. A. Thatcher, and J. A. Barras, 2016: Topobathymetric elevation model development using a new methodology: Coastal National Elevation Database. *J. Coastal Res.*, **76**, 75–89, https://doi.org/10.2112/SI76-008.

de Orla-Barile, M., F. Cannon, N. S. Oakley, and F. M. Ralph, 2022: A climatology of narrow cold-frontal rainbands in Southern California. *Geophys. Res. Lett.*, **49**, e2021GL095362, https://doi.org/10.1029/2021GL0953.

Dettinger, M. D., F. M. Ralph, T. Das, P. J. Neiman, and D. R. Cayan, 2011: Atmospheric rivers, floods and the water resources of California. *Water*, **3**, 445–478, https://doi.org/10.3390/w3020445.

Dowell, D. C., and Coauthors, 2022: The High-Resolution Rapid Refresh (HRRR): An hourly updating convection-allowing forecast model. Part I: Motivation and system description. *Wea. Forecasting*, **37**, 1371–1395, https://doi.org/10.1175/WAF-D-21-0151.1.

English, J. M., D. D. Turner, T. I. Alcott, W. R. Moninger, J. L. Bytheway, R. Cifelli, and M. Marquis, 2021: Evaluating operational and experimental HRRR model forecasts of atmospheric river events in California. *Wea. Forecasting*, **36**, 1925–1944, https://doi.org/10.1175/WAF-D-21-0081.1.

FEMA, 2019a: California severe winter storms, flooding, landslides, and mudslides: DR-4431-CA. FEMA, www.fema.gov/disaster/4431.

——, 2019b: California severe winter storms, flooding, landslides, and mudslides: DR-DR-4434-CA. FEMA, www.fema.gov/disaster/4434.

Gochis, D. J., and Coauthors, 2021: The NCAR WRF-Hydro modeling system technical description, version 5.2.0. NCAR Tech. Note, 107 pp.

Gupta, H. V., H. Kling, K. K. Yilmaz, and G. F. Martinez, 2009: Decomposition of the mean squared error and NSE performance criteria: Implications for improving hydrologic modeling. *J. Hydrol.*, **377**, 80–91, https://doi.org/10.1016/j.jhydrol.2009.08.003.

Hartman, B., H. Cutler, M. Shields, and D. D. Turner, 2021: The economic effects of improved precipitation forecasts in the United States due to better commuting decisions. *Growth Change*, **52**, 2149–2171, https://doi.org/10.1111/grow.12542.

Hobbs, P. V., 1978: Organization and structure of clouds and precipitation on the mesoscale and microscale in cyclonic storms. *Rev. Geophys.*, **16**, 741–755, https://doi.org/10.1029/RG016i004p00741.

Jacobs, N. A., 2021: Open innovation and the case for community model development. *Bull. Amer. Meteor. Soc.*, **102**, E2002–E2011, https://doi.org/10.1175/BAMS-D-21-0030.1.

James, E. P., and Coauthors, 2022: The High-Resolution Rapid Refresh (HRRR): An hourly updating convection-allowing forecast model. Part II: Forecast performance. *Wea. Forecasting*, **37**, 1397–1417, https://doi.org/10.1175/waf-d-21-0130.1.

Jeon, H., B. Hartman, H. Cutler, R. Hill, Y. Hu, T. Lu, M. Shields, and D. D. Turner, 2022: Estimating the economic impacts of improved wind speed forecasts in the United States electricity sector. *J. Renewable Sustainable Energy*, **14**, 036101, https://doi.org/10.1063/5.0081905.

Johnson, L. E., R. Cifelli, and A. White, 2020: Benefits of an advanced quantitative precipitation information system. *J. Flood Risk Manage.*, **13**, e12573, https://doi.org/10.1111/jfr3.12573.

Jorgensen, D. P., M. N. Hanshaw, K. M. Schmidt, J. L. Laber, D. M. Staley, J. W. Kean, and P. J. Restrepo, 2011: Value of a dual-polarized gap-filling radar in support of Southern California post-fire debris-flow warnings. *J. Hydrometeor.*, **12**, 1581–1595, https://doi.org/10.1175/JHM-D-11-05.1.

Kim, D., B. Nelson, and D.-J. Seo, 2009: Characteristics of reprocessed Hydrometeorological Automated Data System (HADS) hourly precipitation data. *Wea. Forecasting*, **24**, 1287–1296, https://doi.org/10.1175/2009WAF2222227.1.

Ma, Y., V. Chandrasekar, H. Chen, and R. Cifelli, 2021: Quantifying the potential of AQPI gap-filling radar network for streamflow simulation through a WRF-Hydro experiment. *J. Hydrometeor.*, **22**, 1869–1882, https://doi.org/10.1175/JHM-D-20-0122.1.

Martyr-Koller, R. C., H. W. J. Kernkamp, A. van Dam, M. van der Wegen, L. V. Lucas, N. Knowles, B. Jaffe, and T. A. Fregoso, 2017: Application of an unstructured 3D finite volume numerical model to flows and salinity dynamics in the San Francisco Bay-delta. *Estuarine Coastal Shelf Sci.*, **192**, 86–107, https://doi.org/10.1016/j.ecss.2017.04.024.

Matrosov, S. Y., D. E. Kingsmill, B. E. Martner, and F. M. Ralph, 2005: The utility of X-band polarimetric radar for continuous quantitative estimates of rainfall parameters. *J. Hydrometeor.*, **6**, 248–262, https://doi.org/10.1175/JHM424.1.

Miller, P. A., M. F. Barth, and L. Benjamin, 2005: An update on MADIS observation ingest integration, quality control, and distribution capabilities. *21st Int. Conf. on Interactive Information and Processing Systems for Meteorology, Oceanography, and Hydrology*, San Diego, CA, Amer. Meteor. Soc., J7.12, https://ams.confex.com/ams/Annual2005/techprogram/paper_86703.htm.

Nash, J. E., and J. V. Sutcliffe, 1970: River flow forecasting through conceptual models. Part I—A discussion of principles. *J. Hydrol.*, **10**, 282–290, https://doi.org/10.1016/0022-1694(70)90255-6.

NCEI, 2021: U.S. billion-dollar weather and climate disasters. NOAA, www.ncdc.noaa.gov/billions/.

Nederhoff, K., R. Saleh, B. Tehranirad, L. Herdman, L. Erikson, P. L. Barnard, and M. van der Wegen, 2021: Drivers of extreme water levels in a large, urban,

high-energy coastal estuary—A case study of the San Francisco Bay. *Coastal Eng.*, **170**, 103984, https://doi.org/10.1016/j.coastaleng.2021.103984.

Neiman, P. J., F. M. Ralph, A. B. White, and D. E. Kingsmill, 2002: The statistical relationship between upslope flow and rainfall in California's coastal mountains: Observations during CALJET. *Mon. Wea. Rev.*, **130**, 1468–1492, https://doi.org/10.1175/1520-0493(2002)130<1468:TSRBUF>2.0.CO;2.

Niu, G., and Coauthors, 2011: The community Noah land surface model with multi-parameterization options (Noah-MP): 1. Model description and evaluation with local-scale measurements. *J. Geophys. Res.*, **116**, D12109, https://doi.org/10.1029/2010JD015139.

NOAA Science Advisory Board, 2021: A report on priorities for weather research. NOAA Science Advisory Board Rep., 119 pp., https://sab.noaa.gov/wp-content/uploads/2021/12/PWR-Report_Final_12-9-21.pdf.

Ralph, F. M., J. J. Rutz, J. M. Cordeira, M. Dettinger, M. Anderson, D. Reynolds, L. J. Schick, and C. Smallcomb, 2019: A scale to characterize the strength and impacts of atmospheric rivers. *Bull. Amer. Meteor. Soc.*, **100**, 269–289, https://doi.org/10.1175/BAMS-D-18-0023.1.

Ray, A. J., and A. B. White, 2019: The Hydrometeorology Testbed–West legacy observing network: Supporting research to applications for atmospheric rivers and beyond. *Atmosphere*, **10**, 533, https://doi.org/10.3390/atmos10090533.

Rutledge, S. A., V. Chandrasekar, B. Fuchs, J. George, F. Junyent, B. Dolan, P. C. Kennedy, and K. Drushka, 2019: SEA-POL goes to sea. *Bull. Amer. Meteor. Soc.*, **100**, 2285–2301, https://doi.org/10.1175/BAMS-D-18-0233.1.

Ruzanski, E., V. Chandrasekar, and Y. Wang, 2011: The CASA nowcasting system. *J. Atmos. Oceanic Technol.*, **28**, 640–655, https://doi.org/10.1175/2011JTECHA1496.1.

Sumargo, E., and Coauthors, 2020: The hydrometeorological observation network in California's Russian River watershed: Development, characteristics, and key findings from 1997 to 2019. *Bull. Amer. Meteor. Soc.*, **101**, E1781–E1800, https://doi.org/10.1175/BAMS-D-19-0253.1.

Tehranirad, B., L. Herdman, K. Nederhoff, L. Erikson, R. Cifelli, G. Pratt, M. Leon, and P. Barnard, 2020: Effect of fluvial discharges and remote non-tidal residuals on compound flood forecasting in San Francisco Bay. *Water*, **12**, 2481, https://doi.org/10.3390/w12092481.

Turner, D. D., H. Cutler, M. Shields, R. Hill, B. Hartman, Y. Hu, T. Lu, and H. Jeon, 2022: Evaluating the economic impacts of improvements to the High-Resolution Rapid Refresh (HRRR) numerical weather prediction model. *Bull. Amer. Meteor. Soc.*, **103**, E198–E211, https://doi.org/10.1175/BAMS-D-20-0099.1.

White, A. B., P. J. Neiman, F. M. Ralph, D. E. Kingsmill, and P. O. G. Persson, 2003: Coastal orographic rainfall processes observed by radar during the California Land-Falling Jets Experiment. *J. Hydrometeor.*, **4**, 264–282, https://doi.org/10.1175/1525-7541(2003)4<264:CORPOB>2.0.CO;2.

——, and Coauthors, 2013: A twenty-first-century California observing network for monitoring extreme weather events. *J. Atmos. Oceanic Technol.*, **30**, 1585–1603, https://doi.org/10.1175/JTECH-D-12-00217.1.

——, K. M. Mahoney, and R. Cifelli, 2015: Wind profilers to aid with monitoring and forecasting of high-impact weather in the southeastern and western United States. *Bull. Amer. Meteor. Soc.*, **96**, 2039–2043, https://doi.org/10.1175/BAMS-D-14-00170.1.

——, B. J. Moore, D. J. Gottas, and P. J. Neiman, 2019: Winter storm conditions leading to excessive runoff above California's Oroville Dam during January and February 2017. *Bull. Amer. Meteor. Soc.*, **100**, 55–70, https://doi.org/10.1175/BAMS-D-18-0091.1.

Zhang, J., Y. Qi, and D. Kingsmill, 2012: Radar-based quantitative precipitation estimation for the cool season in complex terrain: Case studies from the NOAA Hydrometeorology Testbed. *J. Hydrometeor.*, **13**, 1836–1854, https://doi.org/10.1175/JHM-D-11-0145.1.

——, and Coauthors, 2016: Multi-Radar Multi-Sensor (MRMS) quantitative precipitation estimation: Initial operating capabilities. *Bull. Amer. Meteor. Soc.*, **97**, 621–638, https://doi.org/10.1175/BAMS-D-14-00174.1.

Zhu, Y., and R. E. Newell, 1998: A proposed algorithm for moisture fluxes from atmospheric rivers. *Mon. Wea. Rev.*, **126**, 725–735, https://doi.org/10.1175/1520-0493(1998)126<0725:APAFMF>2.0.CO;2.

Zrnić, D., P. Zhang, V. Melnikov, and D. Mirkovic, 2020: Of fire and smoke plumes, polarimetric radar characteristics. *Atmosphere*, **11**, 363, https://doi.org/10.3390/atmos11040363.